Design and Construction of a Wind Tunnel Model with Active Variable Camber Continuous Trailing Edge Flap for Aeroelastic “In-Flight” Shape Optimization Tests

Nathan Precup

A dissertation

submitted in partial fulfillment of the

requirements for the degree of

Master of Science in Aeronautics & Astronautics

University of Washington

2018

Reading Committee:

Eli Livne, Chair

Carl Knowlen

Program Authorized to Offer Degree:

William E Boeing Department of Aeronautics & Astronautics

University of Washington

Abstract

Design and Construction of a Wind Tunnel Model with Active Variable Camber Continuous Trailing Edge Flap for Aeroelastic "In-Flight" Shape Optimization Tests

Nathan Precup

Chair of the Supervisory Committee:
Professor Eli Livne
William E Boeing Department of Aeronautics & Astronautics

An aeroelastically scaled wing wind tunnel model was designed and fabricated for low-speed wind tunnel tests of real-time optimization-based continuous camber and twist shaping concepts for the SSCI-DIRECT project. The model has twelve independently controlled trailing edge control surfaces that can be actively driven while testing is underway. Development of the model follows the successful development and wind tunnel tests of smaller VCCTEF configured aeroelastic models which were fitted with manually adjusted flaps. The new active model packages the flap actuators completely within the outer mold line of the wing. Detailed analytical models for the structural dynamic and aeroelastic behavior of the new model were validated by static loads and modal tests. Wind tunnel runs were carried out to measure lift and drag characteristics of the new model and to gain experience with its continuous communication with the data acquisition system of the wind tunnel and the control algorithms. The wind tunnel model is available for further testing.

TABLE OF CONTENTS

LIST OF FIGURES

LIST OF TABLES

ACKNOWLEDGEMENTS

The support of Dr. Nhan Nguyen and his team at NASA Ames research center, Dr. Jovan Boskovic at Scientific Systems Company, Inc. (SSCI), and Prof. Livne's Boeing Endowed Aeronautics and Astronautics Professorship, made this project possible. Marat Mor provided NASTRAN analysis work and expertise. Thanks to Eliot George and Fiona Spencer at the University of Washington William E. Boeing Department of Aeronautics and Astronautics. At the Kirsten Wind Tunnel: many thanks to Carl Knowlen and the student crew. Thanks also to Tyler Mundt, Casey Chandler, and Kyle Nyberg. Aeronautical Testing Service, Inc. (ATS) provided design advice and manufacturing support.

1. INTRODUCTION

The Variable Camber Continuous Trailing Edge Flap wing concept (VCCTEF) has been studied by NASA for quite some time for its potential to improve efficiency of flight vehicles by optimally shaping their wings in flight in response to changing flight conditions and using a palette of wing shapes much richer than what current technology offers [1]. A historical perspective on the development of this technology can be found in the introductions and bibliographies of references [1] and [2]. As part of the SSCI Phase II DIRECT project the University of Washington was tasked with the design and fabrication of an aeroelastically scaled wing model for low-speed wind tunnel tests of this technology. In two earlier projects for Boeing and NASA [2]-[4], the University of Washington's Kirsten Wind Tunnel (KWT) developed static-aeroelastically scaled VCCTEF-configured models and tested them in the KWT over a range of flight conditions, root angles of attack, and shapes of the VCCTEF (Figure 2). The geometry of the wings was that of the GTM (Generic Transport Model) similar in class to the Boeing 757. Their stiffness was reduced to represent the stiffness of modern composite optimized wings. The multiple segments of the VCCTEF were placed at pre-selected desired angles by hand using mechanical guides. Efficiency of operation of the KWT and its crew led to the collection of a significant amount of data for subsequent correlation with evolving numerical analysis and optimization capabilities.

A natural step forward in the development of VCCTEF technology was to develop the algorithms for optimal active wing camber and twist shaping using VCCTEF's multiple-segments when a control system communicates directly with the airplane. Real time measurements of lift and drag forces, angle of attack, and positions of control surface segments are used by an optimization algorithm, that works, subject to constraints, to optimize the shape of the VCCTEF and drive its segments for maximizing or minimizing some objective function or a combination of objective functions.

To gain experience with such real-time optimization-driven active control, an active aeroelastic model, representative of state of the art commercial aircraft wing designs, was required. The geometry of the wind tunnel model was based on the now widely used and public domain NASA's Common Research Model (CRM) [5][6] with spanwise flexibility that would represent current flexible commercial aircraft and with a jig shape that would lead to optimal design-condition performance in the wind tunnel in the clean wing configurations. The new model was to be larger than the earlier VCCTEF-configured GTM models, to be tested horizontally on the side-wall balance of the KWT.

Figure 1: Front view of the clean wing GTM VCCTEF aeroelastic model at the KWT

Figure 2: The high-lift GTM based VCCTEF aeroelastic wing model at the KWT

2. WIND TUNNEL MODEL DESIGN

To accomplish the goal of this project, a brand new wing planform and design did not need to be created from the ground up. Yet the model also does not need to be based on any wing currently in service, and that allowed certain design freedoms. Aeroelastic scaling did not have to match a well defined structure. The only aeroelastic criteria the wing was required to match is an approximately 10% of span vertical deflection of the wing tip at cruise condition. This deflection is representative of a modern composite commercial transport aircraft wing.

The GTM was used for the previous projects, but for the new project there were several reasons to move to a new design. The GTM is not a modern design, and previous models were not optimized for their aeroelastic deflection in the tunnel. It is also proprietary, and cannot be openly shared by the research community. The Common Research Model (CRM), however, is open, was developed using state of the art design tools, and is being actively used by the research community. For these reasons the CRM was selected as the platform to base the wind tunnel model off [5][6].

The CRM geometry is available for use in ‘1G cruise’ configuration, with no structural design, and a wing shape with a more typical wing deflection of a conventional aluminum wing structure. Because we are increasing the flexibility of the swept wing and targeting a larger wing deflection in the wind tunnel, the lift distribution of the model will be altered. We required the computation of a jig shape twist that would provide optimal or close to optimal wing performance at a wind tunnel design condition of 20psf and CL=0.5. The goal was to start with a design that was optimized for a given wind tunnel condition and test an optimization algorithm at points at and around that optimal wind tunnel condition. To determine the desired wing shape, the CRM geometry was flattened (airfoil sections were rotated to 0° angle of incidence and translated vertically to create a flat wing). A CFD-based optimization was performed on the flattened geometry by NASA to create the jig-shape twist that produced the optimum lift/drag ratio at the design flight condition (Figure 3).

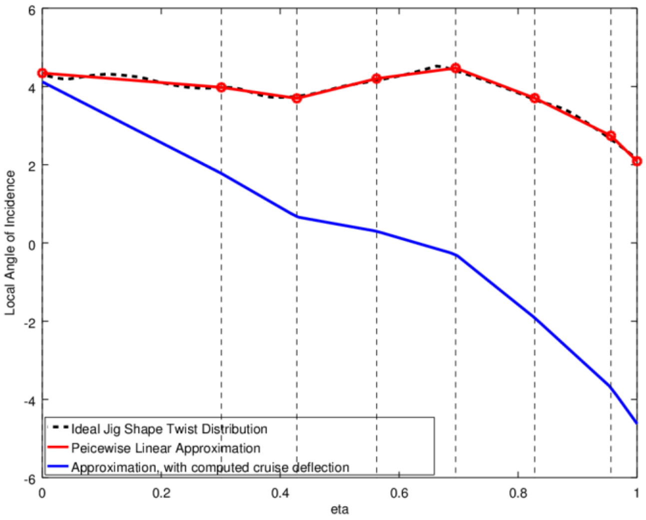

Figure 3: Optimized Jig-Shape Twist Distribution and Estimated Twist Distribution at 1G Cruise Deflection

For optimal drag evaluation, a smooth continuous skin surface was desired. Conventional aeroelastic wind tunnel models are usually based on a stiffness-tailored internal spar with attached masses, covered by segmented airfoil-shape fairings. The gaps between fairing sections are sources of drag. In the design described here an effort was made to remove unrepresentative sources of drag, for a more realistic evaluation of the VCCTEF system. A fiberglass wing with foam core is a simple construction technique that can be tailored to match the desired stiffness and has a smooth aerodynamic surface. Vortex shedding of flap segments set at different angles was minimized through the use of flexible "smooth" transition strips between neighboring flap segments in the spanwise direction). The transition strips also help to approximate an infinitely variable spanwise flap deflection distribution, even though the number of independent flap segments would have to remain small for practical purposes. A conforming transition strip is also utilized in VCCTEF concepts developed for full scale aircraft.

To provide fine control of the lift distribution, 12 VCCTEF segments would be used, independently actuated, with actuation and deflection measurement system that would be fully enclosed within the outer mold line of the clean wing. The VCCTEF elements are divided into 6 spanwise sections, each with two flap segments. To support this, as large a wing as possible was desired. This size was constrained by the dimensions of the Kirsten Wind Tunnel (8 feet tall, 12 feet wide), as well as the balance loads limitations. The main external balance (floor mounted) would only be practical for a 5 to 6 foot span wing, so the sidewall mounted external balance was selected. This would permit a very large wing, provided the forces do not overload the rolling moment limit of the balance. A wing span of 7 feet was selected as a compromise between scale, balance limitations, and practicality of manufacturing. Overall dimensions are provided in Table 1.

Table 1: Wing Geometry

Wing span (root to tip)	85 inches
Location of Yehudi break	25 inches
Root chord	38.1 inches
Tip chord	8.8 inches
Chord at Yehudi break	23.25 inches
LE sweep	37 degrees
Wing area	12 sq. ft.

Based on NASTRAN prediction and prior experience with the clean wing and high-lift GTM based models, four layers of lightweight 1.5 ounce plain weave fiberglass was used for the skin (fiberglass style 108). The warp and fill fiber orientations were laid at alternating 45 degree angles to the elastic axis, which provides maximum flexibility along the elastic axis. The foam core was CNC cut from extruded polystyrene foam. Flap segments and balance connections needed to be manufactured to tight tolerance with high strength. Reinforcement at the root of the wing and the twelve actuated sections were made using 6061 aluminum. The structural layout is shown in Figure 3 along with the naming convention for each actuated section. Each pair of sections has a number, corresponding to the distance from the wing's root, from one (root) to six (tip). The 6 forward segments connected to the wing are referenced as segment A, while the 6 aft segments at the trailing edge were referenced as B. Thus, the sections are labeled, starting from the root moving aft and outboard, 1A, 1B, 2A, 2B, … , 6B. Figure 4 shows an exploded view of all the parts of the wing.

The wing was rigidly attached to the wind tunnel sidewall balance via a steel strut pinned and bolted to the load block shown in Figure 3. The load block was machined from 6061 aluminum, and provided substantial structure for mounting to the wind tunnel balance. It also provided a large surface area for bonding to the fiberglass skin at the wing root, producing a very strong structural attachment point to the wind tunnel balance. Some flap control electronics were also located inside the load block under a cover plate.

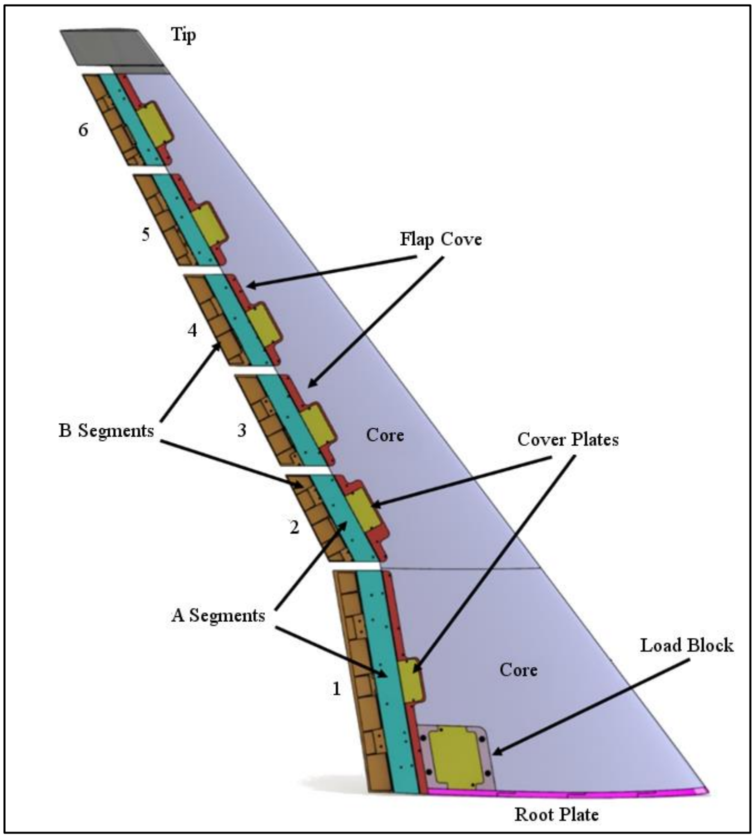

Figure 4: Annotated bottom view of aeroelastic wing CAD model

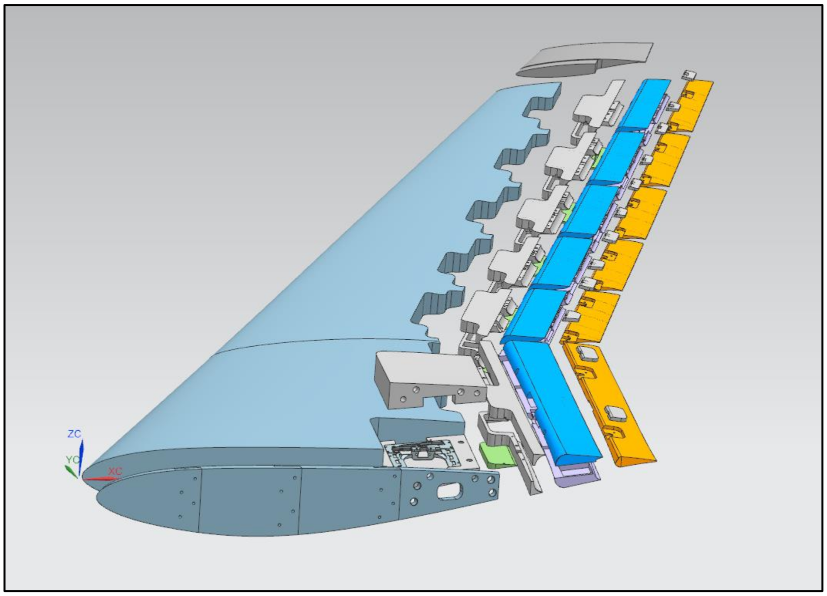

Figure 5: A 3D CAD exploded view of the wind tunnel model

The following series of photos shows the wing installed on the side-wall balance at the KWT:

Figure 6: The wing on the sidewall balance next to the boundary layer splitter plate – top view

Figure 7: The wing on the sidewall balance next to the boundary layer splitter plate – rear view

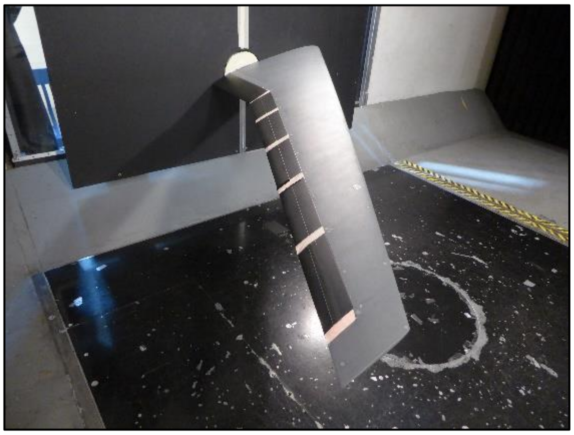

Figure 8: The wing model in the KWT's test section

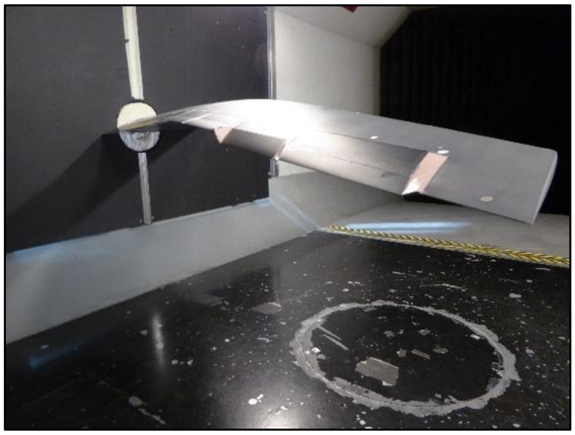

Figure 9: Deformed Silicone/Rubber spanwise strips due to relative motions of spanwise segments

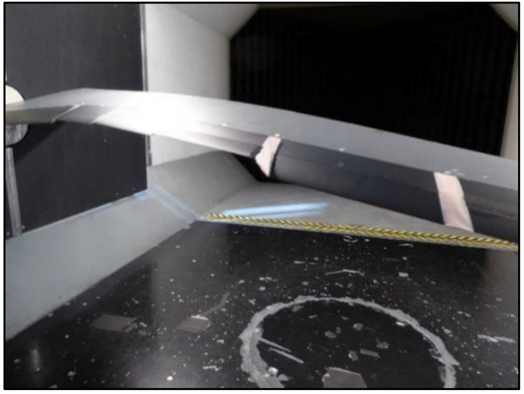

Figure 10: Stretched silicone/rubber spanwise strips due to relative motions of spanwise segments

3. FLAP ACTUATORS

The flap actuation proved to be the most challenging aspect of model design. The design requirement of no external protuberances meant all actuation needed to be packaged inside the outer mold line of the wing. Linear actuation by a lead screw was selected in order to keep all parts within the wing (no control horns). To keep control simple, off-the-shelf thin-wing servos were modified to function as continuous rotation servo. The servo output spline was fitted with a threaded rod for the lead screw. Figure 11 and Figure 12 show the design of the actuators packaged within the OML of the wing.

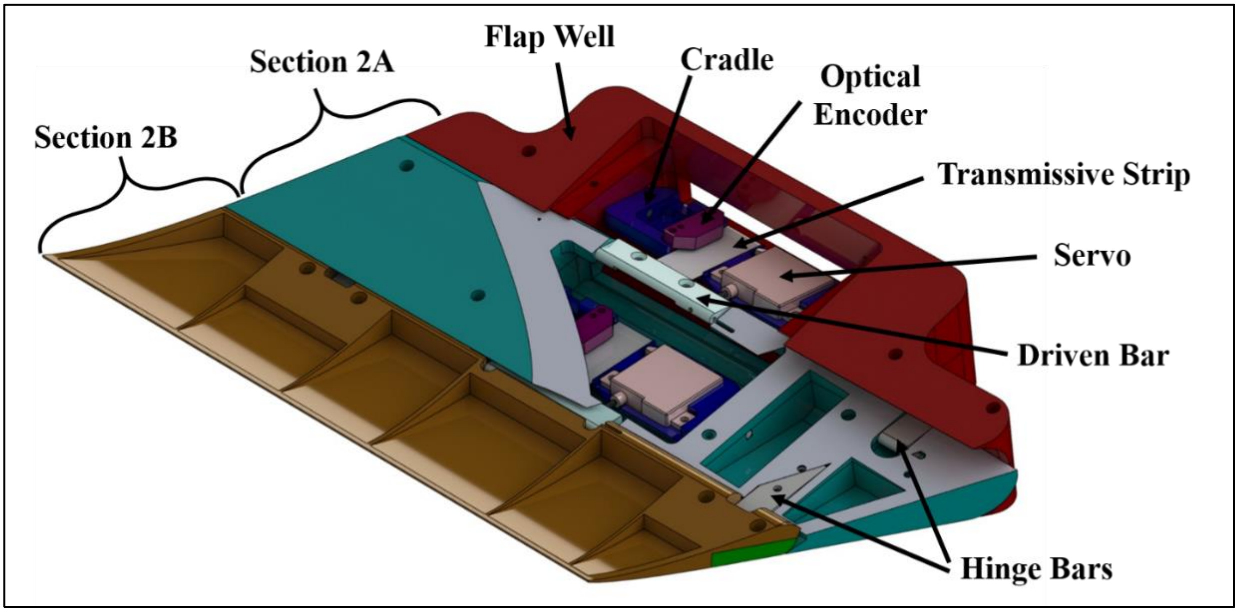

Figure 11: Annotated image of actuator for flap 2A and 2B with select covers removed or cut away

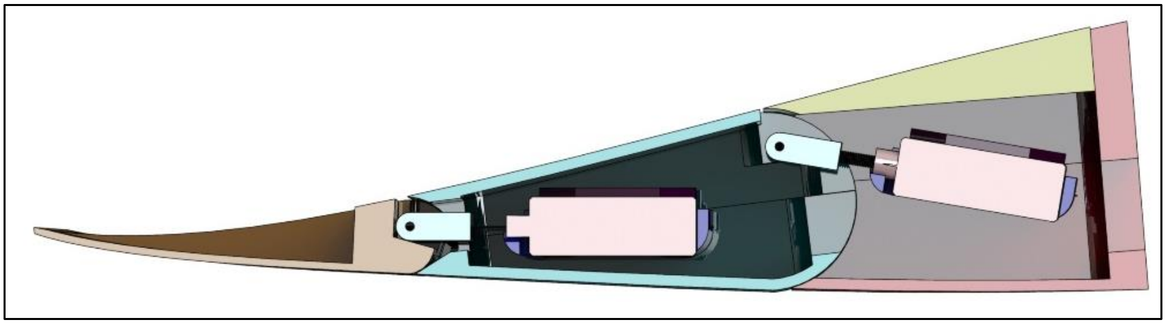

Figure 12: Cutaway view of actuation system for flap 2A and 2B

Control signals to the servos are pulse-width-modulated (PWM) signals. Varying the duty cycle produces direct control of the rotation rate of the modified servos. Initially, Spektrum A7050 thin-wing servos were selected. After the wing was assembled, these servos proved to be inadequate for this application in the way they were used (no control horns). The A7050 servos did not have a full metal body, and stresses from the lead screw produced cracking of the servo housing. Motor burnout was also a problem while running these servos continuously. After identifying the problems with the A7050 servos, they were replaced with MKS HV6130 servos. These all-metal servos are nearly the same size, but have more power and were found to be much more reliable for the application here.

The modification of the servos to function with continuous rotation required disabling the internal closed-loop feedback potentiometer, replacing it with two fixed 2.55 kΩ resistors. To close the loop a feedback sensor was required to measure the deflection of the flap directly. Very fine resolution is necessary to resolve the angle deflection. Extension of the linear actuator is very small, as the radius from the hinge point to the linear actuator attachment is very small, as low as 0.125 inches. US Digital EM2 optical quadrature encoders support a resolution of 0.000125 inches, which produces an angular resolution better than 0.1 degrees. As these optical encoder transmissive strips are very thin, they are relatively easy to package inside the wing and they were selected as the feedback devices for servo control. In actual practice, the accuracy of the measurement was typically on the order of 1 degree, and for very small control arm radii, up to 3 degrees. This uncertainty is due to mechanical backlash and manufacturing tolerances of the hinges, as well as unanticipated axial misalignment of the servo lead screw causing lateral motion and warping of the transmissive strip. The former was significantly more prevalent when commands for small angle adjustments (less than a degree) were sent to the servos in a direction that required motion in the direction opposite of the last command. The latter issue could often be fixed through adjustment of the strip's mounting once the problem was noticed. Furthermore, re-indexing the zero position of bays periodically during testing further improved the consistency of commanded positions.

Each actuator was installed in an aluminum cradle, along with the EM2 optical encoder sensor. The entire cradle was pinned inside the wing section directly in front of the segment it was to control (for segment A, it was pinned inside the flap cove, and for segment B it was pinned inside segment A. The lead screw nut was pinned to the controlled segment and the optical transmissive strip was clamped to the lead screw nut.

The spanwise gaps between flap sections were initially spanned by a silicone elastomer to provide a smooth transition. However, the silicone used (Smooth-On Mold-Max 10) proved too stiff in the thicker parts of the transition strips and resisted the actuators too much. The silicone was replaced with a dual-material 3D-printed component. The new strips utilize a hollow rectangular cross section with a rigid Verowhite material as the side mounting surfaces and a rubber-like TangoBlack material as the top and bottom elastic sections. Views of one of these strips can be seen in Figure 13 and Figure 14. The strips were printed on a Stratasys Objet 260 in digital material mode (32 micron layer thickness). These transition strips possessed more compliance and smoother spline at large relative flap deflections than the original cast silicone and aluminum design. In order to reduce the downtime required during repairs, calibrations, and other adjustments, the gap between the pair of sections 6A and 6B to the tip is discontinuous. A set of discontinuous rigid interfaces, made from the same Verowhite material, were used in early comparison tests.

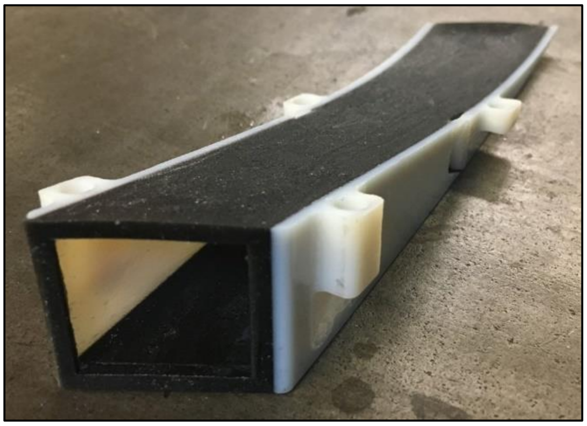

Figure 13: 3D-printed flexible flap transition strip

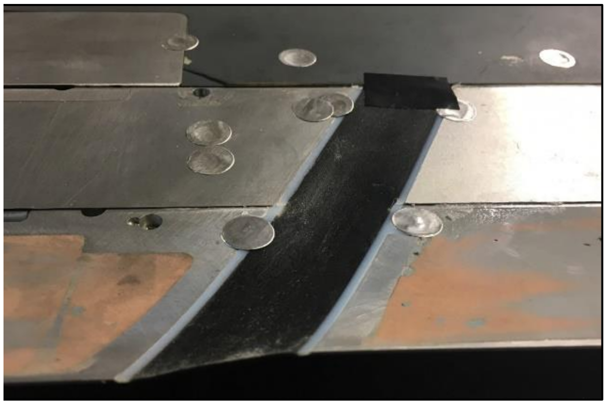

Figure 14: 3D-printed flexible flap transition strip installed between flap sections

4. FLAP CONTROL SYSTEM

The flap control system was developed to provide an abstracted network interface to the individual servos for each VCCTEF segment. This control system offloads the actuator control onto a microcontroller and acts as a networked device for the optimization algorithm to interface with. This wind tunnel model interface is designed to be simple and easy to integrate with any algorithm for wind tunnel testing. Embedded microcontrollers were selected to keep update rates fast, deterministic, and reliable with minimal user interaction. To drive the servos, there must be the capability to set 12 individual PWM signals. To measure the encoders, there must be 12 quadrature encoder counter/timers. For embedded microcontroller systems, this cannot be practically done using the general purpose digital IO. The control system needs dedicated encoder counters and a dedicated PWM source. Two microcontrollers were used to close this feedback loop broken by servo modification, as shown in the system schematic presented in Figure 15.

The first microcontroller, an Arduino Pro Mini (ATmega328), was tasked with the relatively light duty of generating PWM servo control signals and was located within the wing. To produce 12 simultaneous PWM signals of high resolution, a TLC5940 LED driver chip was employed as a peripheral to the Arduino Pro Mini. The TLC5940 is a 16 channel PWM driver with 12-bit resolution of the duty cycle. The Arduino Pro Mini monitors a serial bus to the second microcontroller for updated PWM duty cycle values. This driver circuit and microcontroller was located inside the wing.

The second microcontroller closes the feedback loop by monitoring the encoder positions, comparing them to a target, and sending updated PWM duty cycle values via serial to the Arduino Pro Mini. This second microcontroller is an Arduino Due, a 32-bit ARM processor-based microcontroller with a relatively high 84 MHz clock rate. This microcontroller was selected over a PC based system to ensure deterministic code execution, and to operate without the complexity of a computer with a user interface that needs to be launched on startup. The Arduino Due is housed in a separate control box located outside the wind tunnel test section, and connected to the wind tunnel network to listen for commands. The quadrature encoders at each actuator transmit their signals via a differential line driver (US Digital PC4-H10 driver) to the control box. Twelve LS7366R quadrature encoder counter chips populated on a custom-made mezzanine card convert the quadrature signals into counts. These chips are dedicated counters that can keep up with a 20 MHz quadrature pulse rate. Each one counts encoder quadrature pulses and maintains a 32-bit position value. The Arduino Due reads the 12 encoder values via Serial-Peripheral-Interface (SPI) from each of these encoder counters.

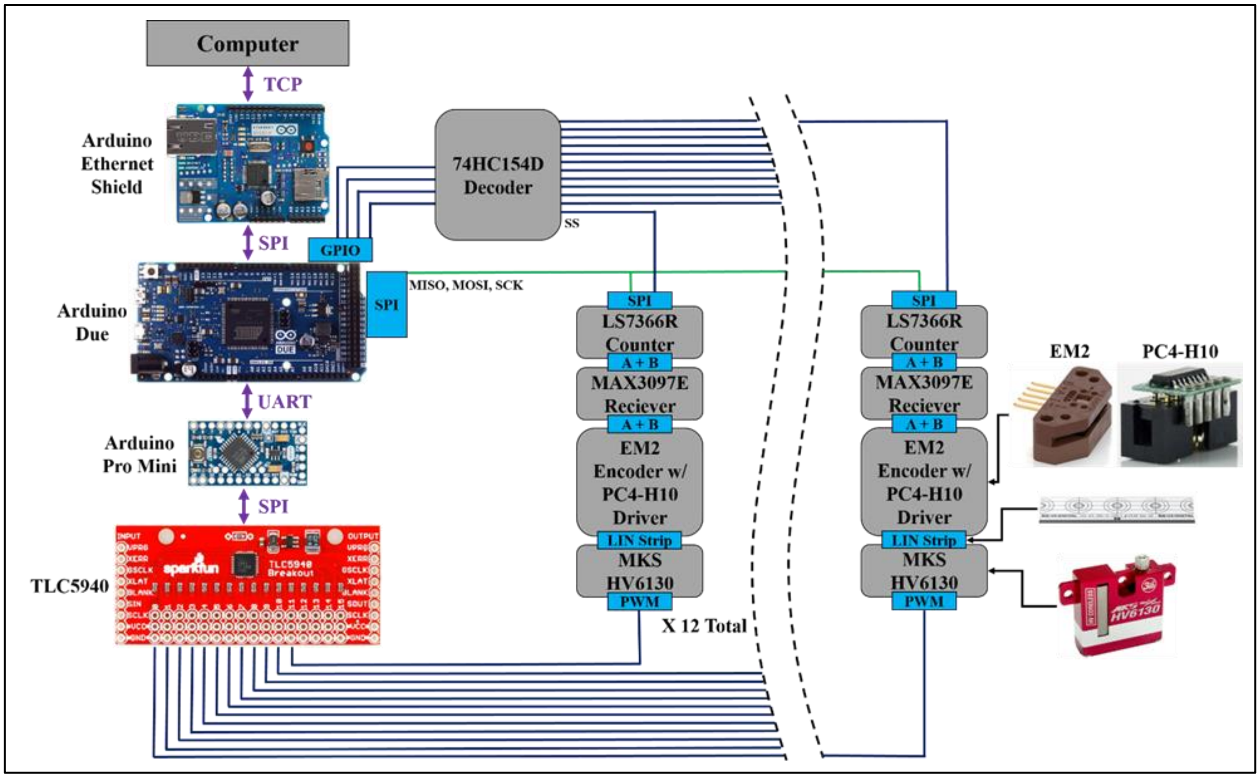

Figure 15: Flap Control System Schematic

A stand-alone windows application was developed using LabVIEW to communicate with the wing without using an optimization algorithm (Figure 16). The software is used for testing and setup purposes. It is also used to calibrate the flap encoders. The encoders are not absolute, and rely on the index mark to properly zero their position on each power cycle. The LabVIEW user interface can be used to drive the flaps to the index point and ensure the wing is prepared for wind-on testing.

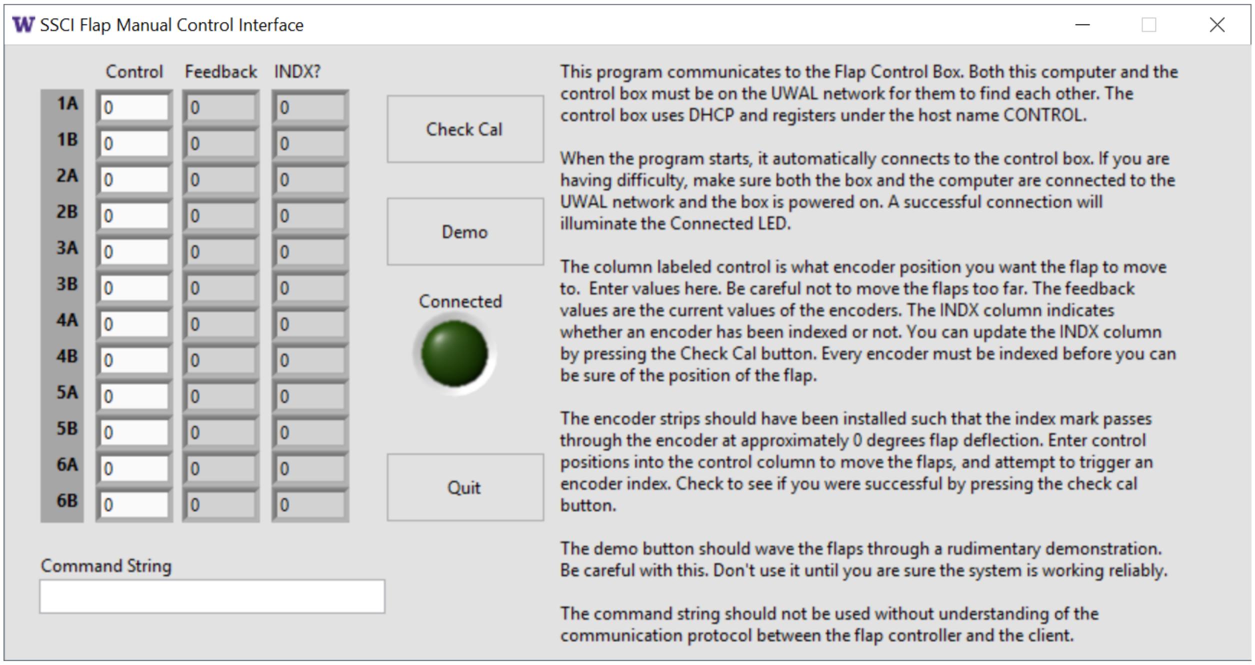

	Control	Feedback	INDX?
1A	0	0	0
1B	0	0	0
2A	0	0	0
2B	0	0	0
3A	0	0	0
3B	0	0	0
4A	0	0	0
4B	0	0	0
5A	0	0	0
5B	0	0	0
6A	0	0	0
6B	0	0	0

This program communicates to the Flap Control Box. Both this computer and the control box must be on the UWAL network for them to find each other. The control box uses DHCP and registers under the host name CONTROL.

When the program starts, it automatically connects to the control box. If you are having difficulty, make sure both the box and the computer are connected to the UWAL network and the box is powered on. A successful connection will illuminate the Connected LED.

The column labeled control is what encoder position you want the flap to move to. Enter values here. Be careful not to move the flaps too far. The feedback values are the current values of the encoders. The INDX column indicates whether an encoder has been indexed or not. You can update the INDX column by pressing the Check Cal button. Every encoder must be indexed before you can be sure of the position of the flap.

The encoder strips should have been installed such that the index mark passes through the encoder at approximately 0 degrees flap deflection. Enter control positions into the control column to move the flaps, and attempt to trigger an encoder index. Check to see if you were successful by pressing the check cal button.

The demo button should wave the flaps through a rudimentary demonstration. Be careful with this. Don't use it until you are sure the system is working reliably.

The command string should not be used without understanding of the communication protocol between the flap controller and the client.

Figure 16: Flap Control User Interface

5. WIND TUNNEL TEST INSTRUMENTATION

Wind tunnel testing incorporates the model mounted to the Kirsten Wind Tunnel’s sidewall balance, which measured the 6 reaction forces and moments. Of particular interest for this experiment were the lift and drag. To alleviate the impact of the wind tunnel wall boundary layer, a boundary layer splitter plate is installed 6 inches off the wall. See Figure 17 for a photo of the splitter plate geometry. The wing is mounted through a hole in the non-metric splitter plate and is rigidly attached to the balance turntable.

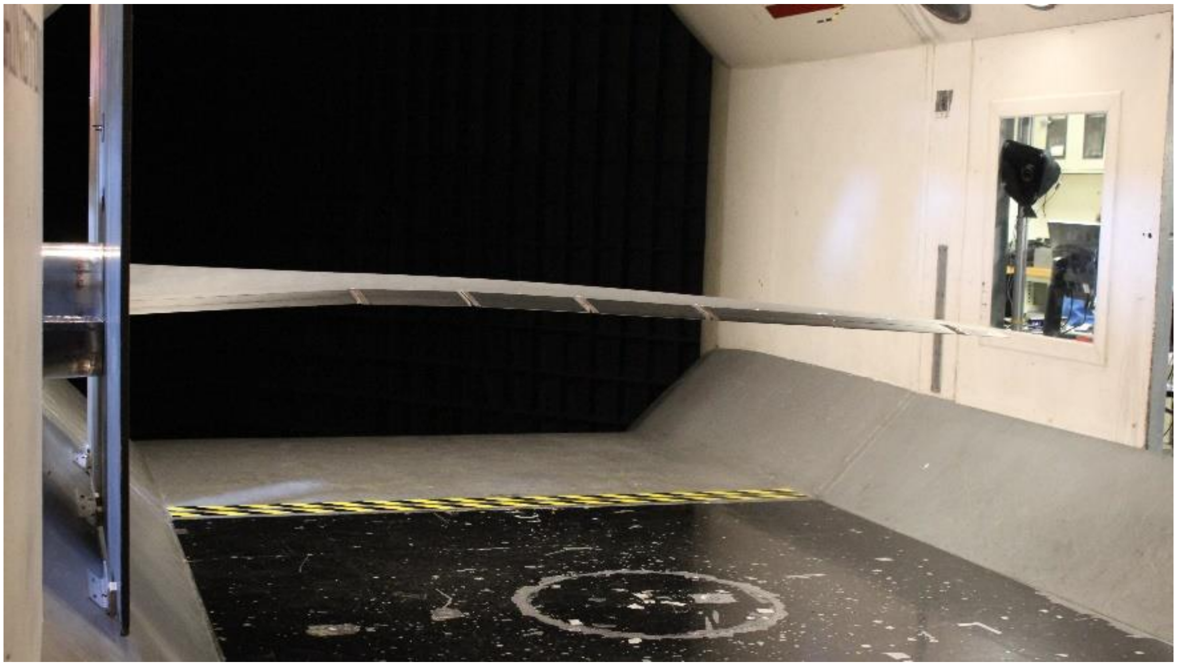

Figure 17: Rear view of CRM installed in KWT on sidewall balance, splitter plate offset shown

A VICON Nexus 3D motion tracking system with 6 VICON Bonita infrared cameras was used to track the position of markers on the wing at 100 Hz. The tracking target locations are shown in Figure 18. This system was used for static load testing and for measuring the wind-on shape of the wing while simultaneously measuring the forces through the wind tunnel balance. The VICON system utilizes a ‘skeleton’ kinematic model, and low-pass filtering to resolve motions of less than 1 mm within the test section volume.

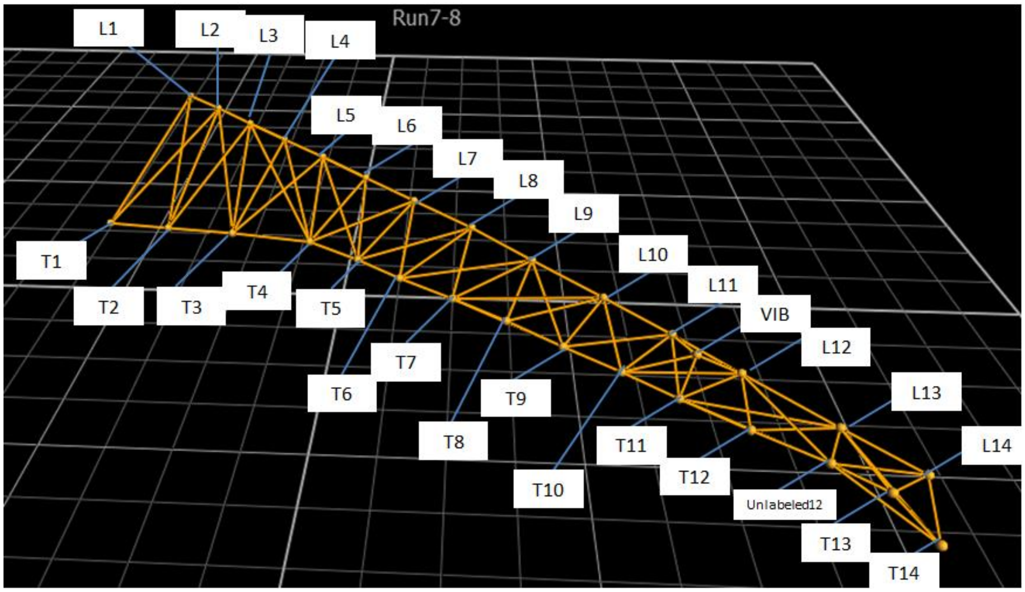

Figure 18: VICON tracking target locations as seen in the VICON Nexus software

The two systems can be synchronized by an LED which is illuminated when the wind tunnel data system is acquiring data for a test point. The VICON system can pick up the sync light as a tracking target. The VICON data file can then be post-processed to compute the averaged locations of each tracking target while the sync light is illuminated. The wind tunnel data system simultaneously records and averages samples of the wind tunnel balance forces, angle of attack, tunnel dynamic and static pressure, and air temperature. Each data point therefore can contain a comprehensive data set of the model orientation, deformation, loads, and tunnel conditions.

A TCP/IP network interface built into the wind tunnel data acquisition system is used to provide real time data streaming to the computer hosting the optimization algorithm. The interface also permits angle of attack commands. The algorithm controller can use a constraint on the lift of the wing, and meet that constraint using a combination of flap and angle of attack adjustments while searching for a drag optimum.

6. AEROELASTIC MATHEMATICAL MODEL DEVELOPMENT

A mathematical model of the new wing system was developed to (a) guide the structural design by making sure that the desired flexibility will be obtained or surpassed, (b) verify, by analysis, ahead of tests, that the model would not flutter nor fail due to static or dynamic loads during the tests, and (c) provide SSCI and NASA with a mathematical model of the system with which they will be able to continue developing their technology based on realistic system information and also prepare for additional future tests using the system for follow-on studies. The modeling work was taken on by Dr. Marat Mor using NASTRAN.

The wing was modally tested three times: wing installed on the sidewall balance resting on the floor without silicone flap transition strips, wing installed on the sidewall balance resting on the floor with the silicone strips, wing installed on the sidewall balance rigidly attached to the KWT test section, with silicone transition strips.

An impact hammer was used to excite the wing. Accelerometers and a laser vibrometer were used to measure response. A Spectral-Dynamics Jaguar system and its software were used for data acquisition and spectral analysis.

In static load tests the wing was loaded by given weights located at various points on the wing. Wing deformation was measured by the Vicon system.

A NASTRAN model was developed for the wing system and fine-tuned by the results of the modal and static tests. Based on the experience gained in the finite element modeling of the type of thin-fiberglass-skin/foam-core structures gained in the development of the earlier VCCTEF wings (Refs. 2 and 3), the NASTRAN model is made of solid, 3D elements to represent the foam and metal parts and plate elements for the skins. Stiff springs are used to represent actuators, soft springs in the spanwise direction represent the spanwise action of the smooth flexible transition strips when the wing bends in fore-aft in-plane motion.

The NASTRAN finite element (FE) model of the wing is shown in the Figure 19 through Figure 21, followed by the correlation between NASTRAN-predicted natural frequencies and measured natural frequencies (Table 2) and figures of mode shapes (Figure 22). The NASTRAN model captures the structural dynamics of the wing quite well.

Correlation of static load test results with predicted NASTRAN results is also good overall. Figure 23 shows load points and deformation measurement points used in the static tests of the model. Figure 24 through Figure 33 show test / analysis correlations.

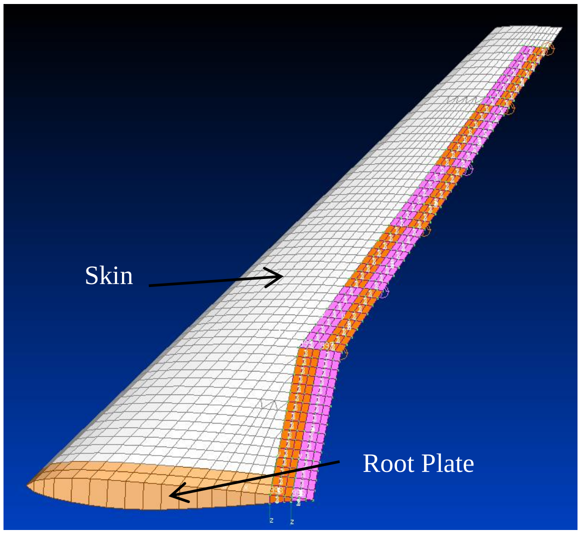

Figure 19: The NASTRAN model: 2D elements

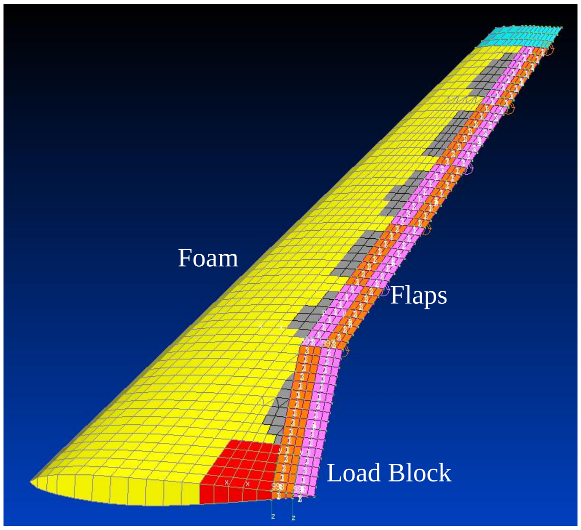

Figure 20: The NASTRAN model: 3D elements

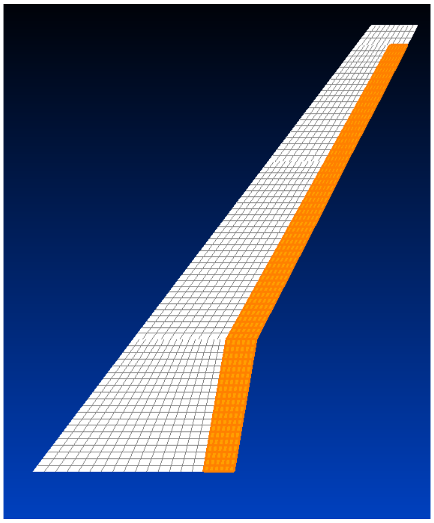

Figure 21: The NASTRAN Model: The Doublet Lattice Mesh

Table 2: Eigenvalue (Natural Frequencies) Test/Analysis comparison

Mode	**Test**	**Nastran**	**Error (%)**	**Description**
1	2.8	2.8	0	1st Bending
2	11.3	12.2	8	2nd Bending
3	13.2	13.0	-1.5	In-Plane Bending + (Vertical) Bending
4	27	31	14.8	Bending + Torsion
5	33	33	0	1st Torsion
6	47	48	2.1	In-Plane Bending
7	52	58	11.5	3rd Bending
8	70	67	-4.3	2nd Torsion
9	-	87	-	4th Bending
10	94	93	1.1	In-Plane Bending + Torsion

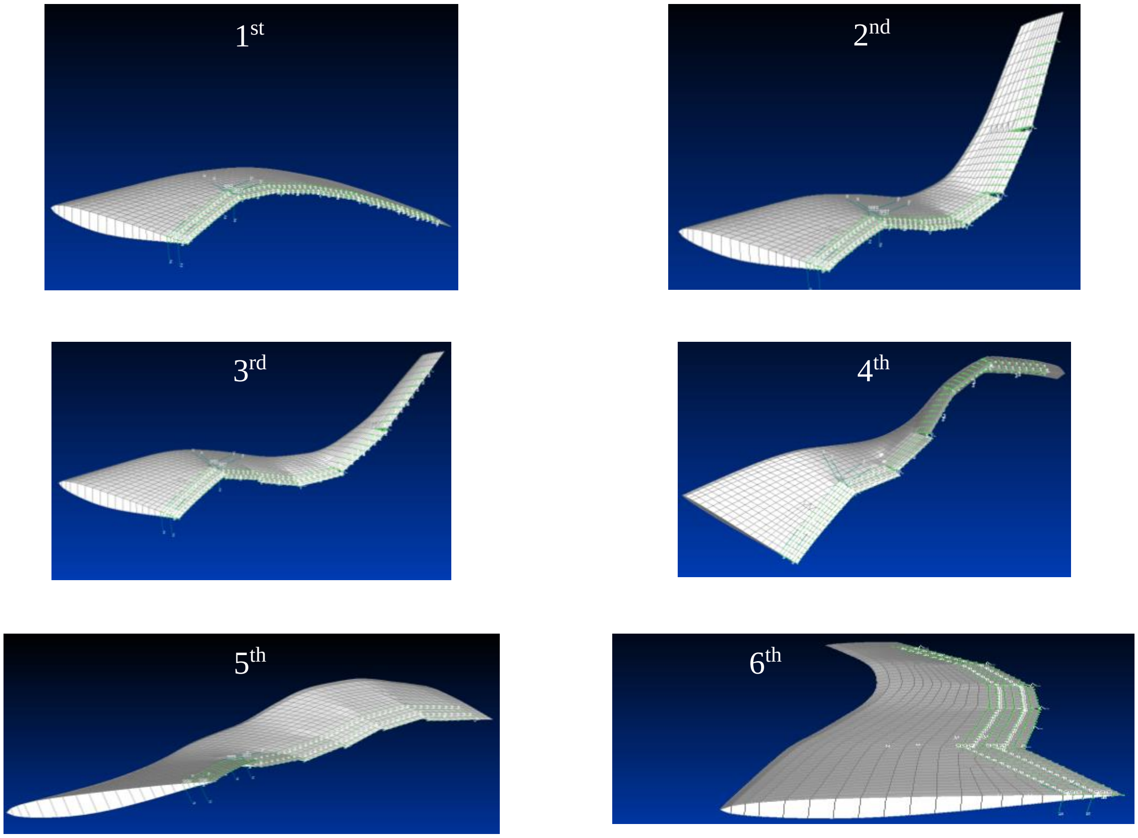

Figure 22: NASTRAN-predicted mode shapes

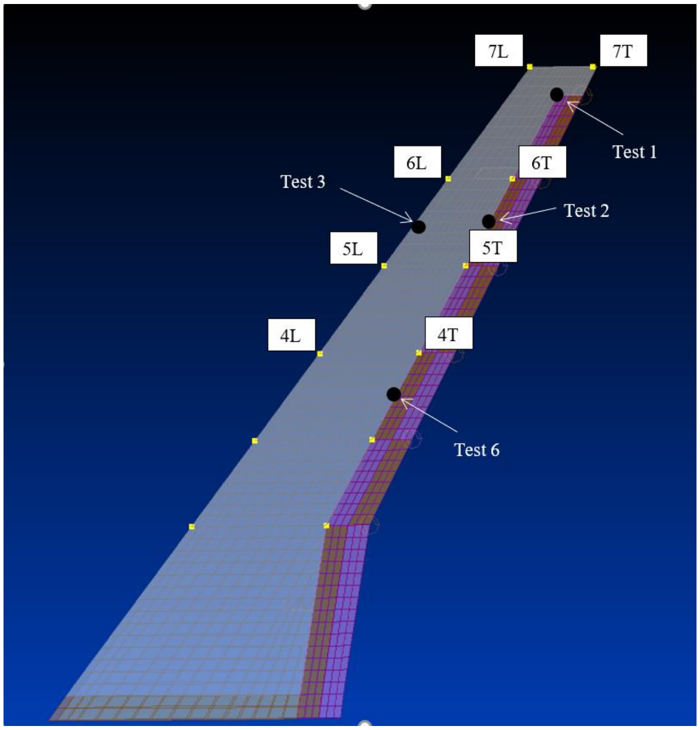

Figure 23: Static Test IDs, Applied Force Locations, and the Locations of Displacement Measurements

Note: Reflective spheres were used for the Vicon system in the static load cases. A different array of reflective dots was used for wind tunnel testing.

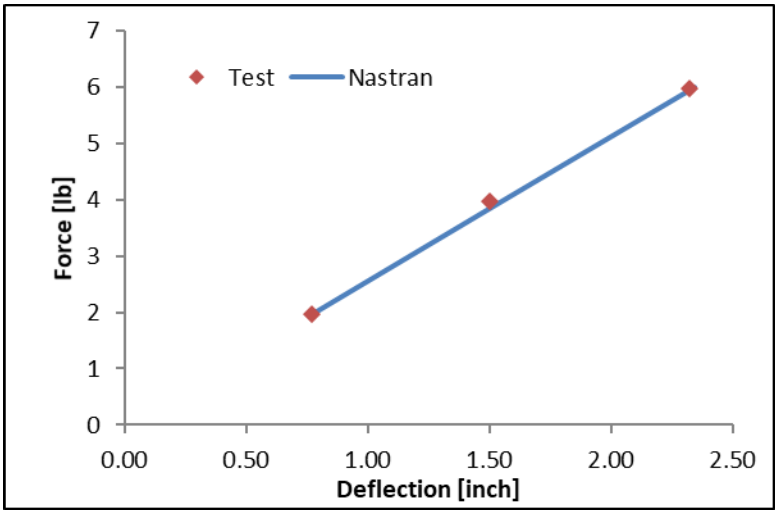

Figure 24: Static Test/NASTRAN Model Correlation: Load Test 1, Output 7L

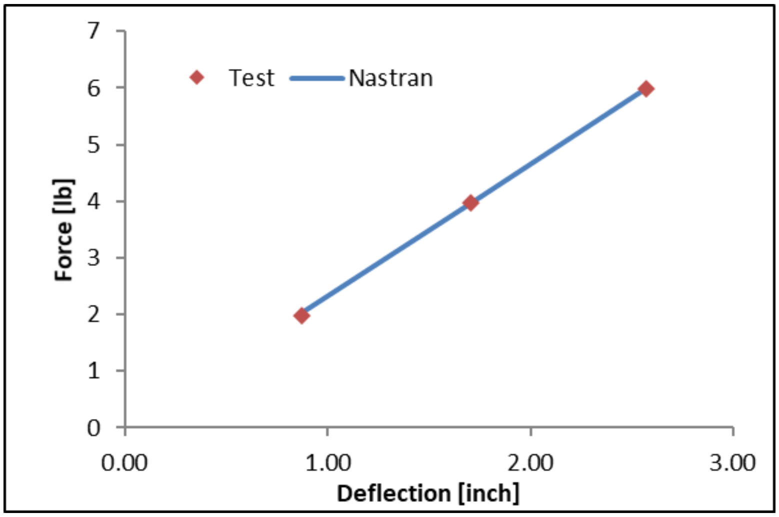

Figure 25: Static Test/NASTRAN Model Correlation: Load Test 1, Output 7T

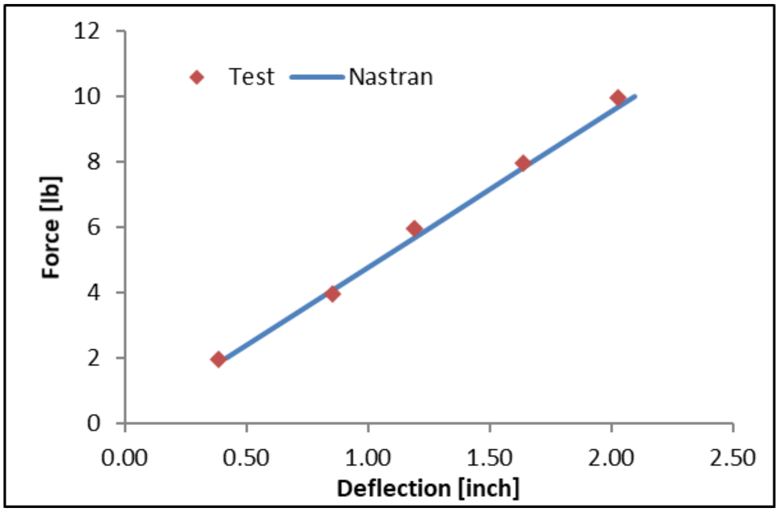

Figure 26: Static Test/NASTRAN Model Correlation: Load Test 2, Output 7L

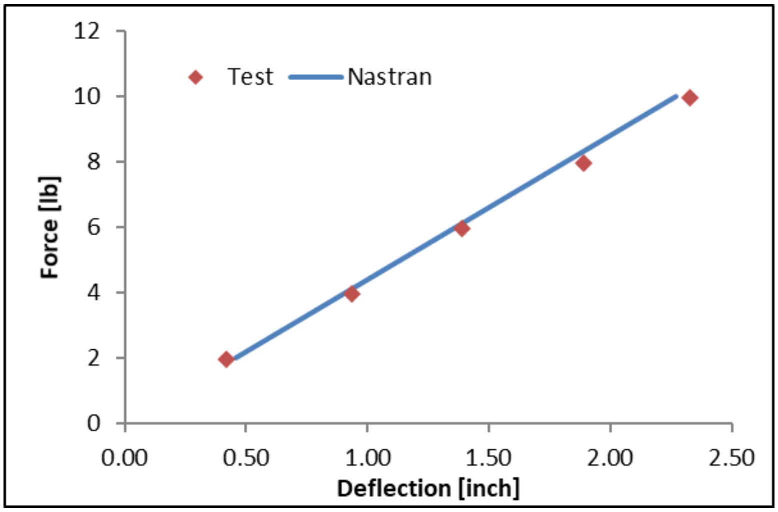

Figure 27: Static Test/NASTRAN Model Correlation: Load Test 2, Output 7T

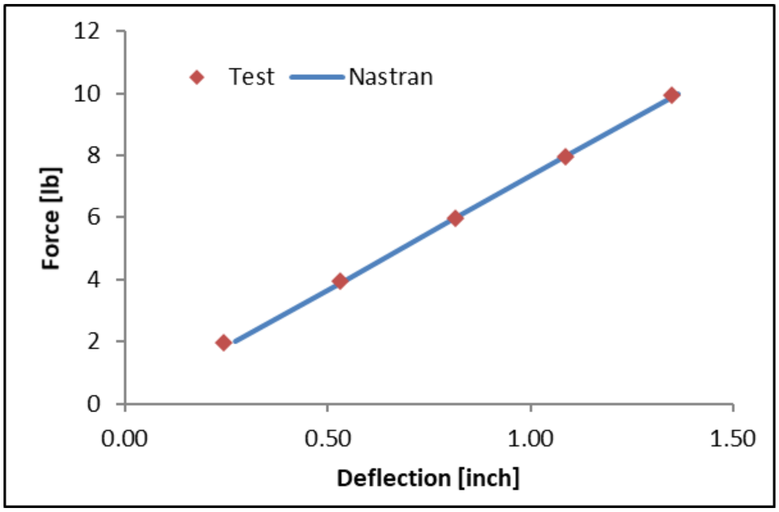

Figure 28: Static Test/NASTRAN Model Correlation: Load Test 2, Output 6L

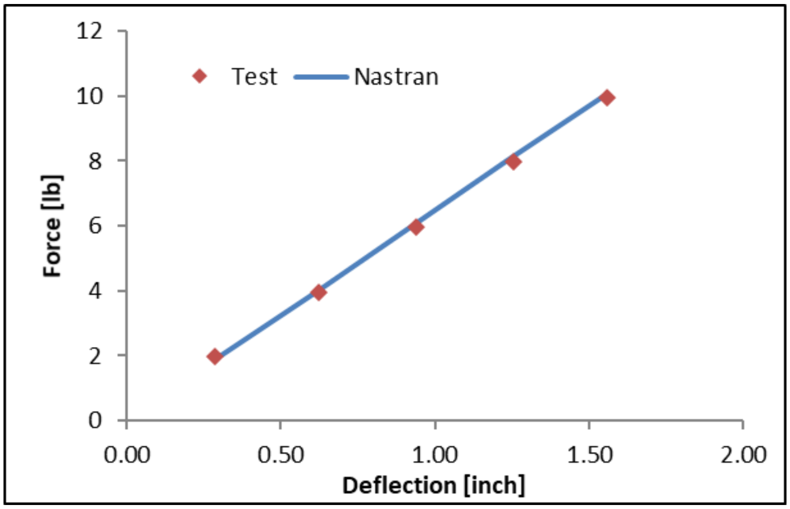

Figure 29: Static Test/NASTRAN Model Correlation: Load Test 2, Output 6T

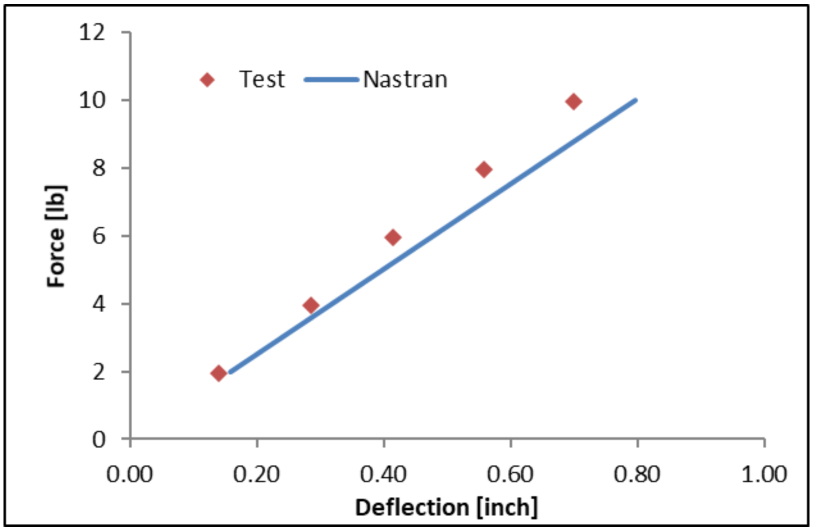

Figure 30: Static Test/NASTRAN Model Correlation: Load Test 3, Output 5L

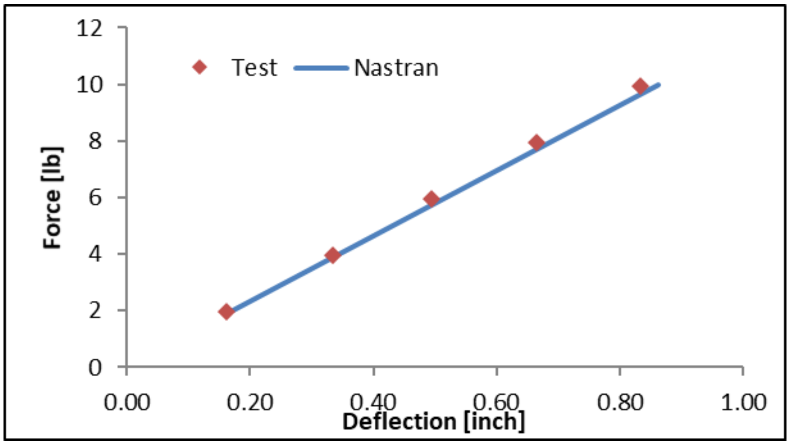

Figure 31: Static Test/NASTRAN Model Correlation: Load Test 3, Output 5T

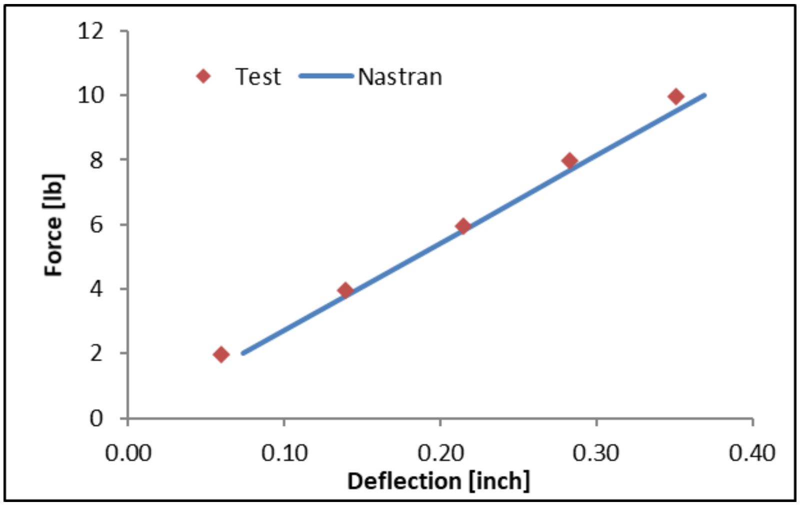

Figure 32: Static Test/NASTRAN Model Correlation: Load Test 3, Output 4L

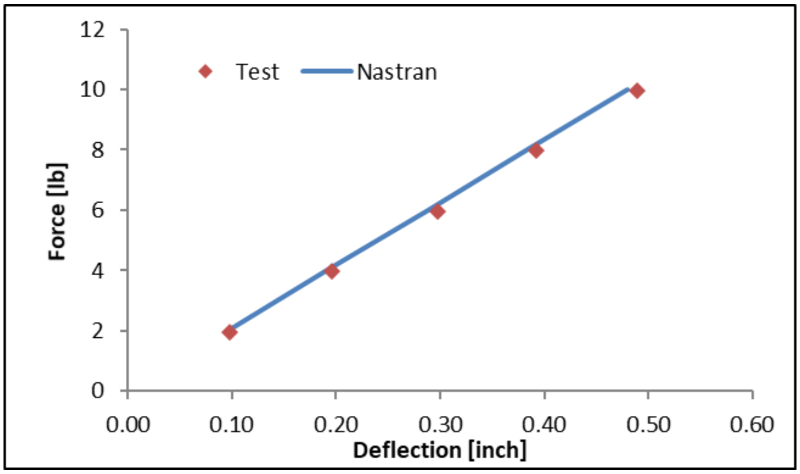

Figure 33: Static Test/NASTRAN Model Correlation: Load Test 3, Output 4T

Flutter predictions for the wing are shown in Table 3.

Table 3: Flutter Predictions

		Flutter [ft/sec]	Flutter Frequency [Hz]	Flutter Mode	2nd Unstable Crossing [ft/sec]	Frequency [Hz]
	No Springs	246	12.3	2nd or 3rd	267	19
	Current	264	13.2	3rd	290	20
Spring between the flaps are increased by a multiple of:	x6	275	14.2	3rd	290	20
	x18	280	14.7	3rd	290	20
	x100	285	15.1	3rd	290	20

To address uncertainty in the stiffness effect of the flap transition strips in the in-plane direction (the strips are very soft in the vertical direction relative to the stiffness of the actuators) a parametric study of the effect of flap transition strip spring stiffness on the flutter results was carried out. In all cases studied the flutter speed of the system is much higher than the maximum dynamic pressure planned for the tests (standard-atmosphere sea level and dynamic pressure of 20 psf, the air speed is 130 ft/sec).

7. WIND TUNNEL TESTING FOR MODEL VALIDATION

Locations and designation of the VICON reflective dots on the model are shown earlier in Figure 18. Figure 34 through Figure 37 show VICON software screen shots with images of the wing at 8 degrees angle of attack wind-off and wind-on at q=15psf. Comparison between wind tunnel testing and NASTRAN aeroelastic trim solution results of the lift coefficient vs angle of attack are shown in Figure 38. NASTRAN captures the linear behavior very well.

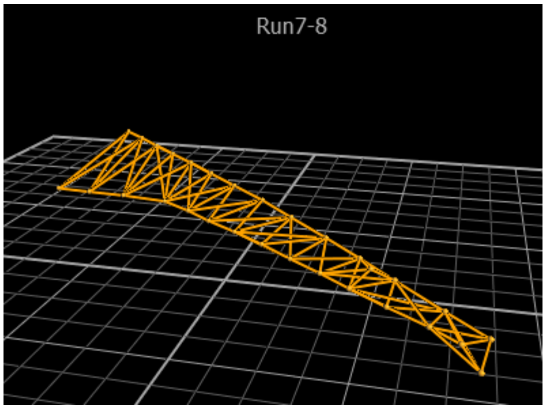

Figure 34: AOA=8deg. Wind off.

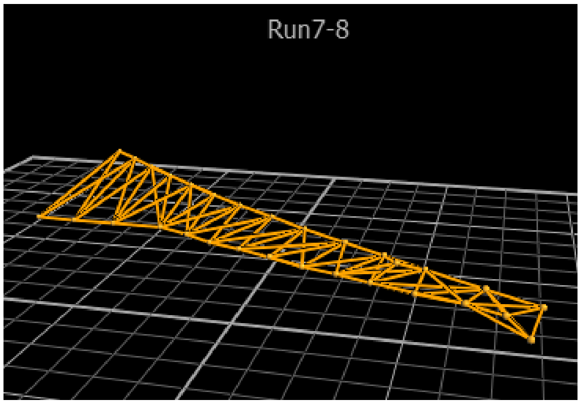

Figure 35: q=15psf, AOA=8deg. Wind on.

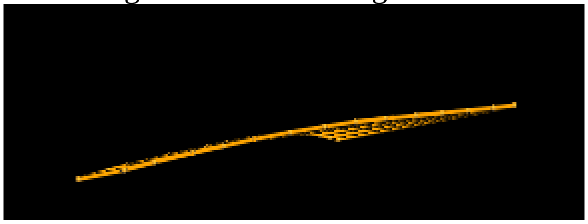

Figure 36: AOA=8 degrees. Wind off. View from the right.

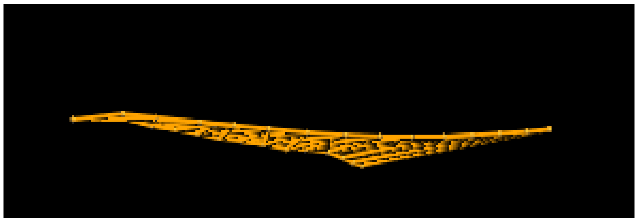

Figure 37: q=15psf, AOA=8 degrees. Wind on. View from the right.

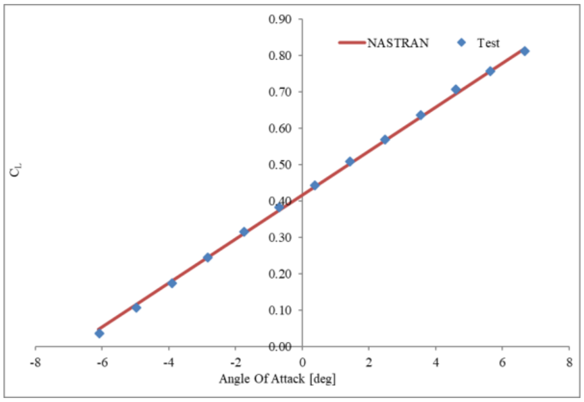

Figure 38: Lift coefficient vs Angle of Attack at dynamic pressure q = 10 psf

8. CHALLENGES & LESSONS LEARNED

There were many challenges faced and lessons learned from this project. For future work expanding on this wind tunnel testing capability, this section will hopefully be a useful guide.

8.1 STRUCTURE & CONSTRUCTION

Overall the construction technique used worked very well. Fiberglass is easy to work with. The extruded polystyrene, while readily available and inexpensive, seems to be the source of structural creep. With the wing installed on the wind tunnel balance horizontally for a period of time, the structure slowly creeps. When removed from the balance and set upright, the wing retains a drooped shape. This is not a fatal flaw, but care must be taken to conduct wind tunnel testing with this in mind. Any change in wind-off shape should be regularly accounted for and subtracted from the wind-on data accordingly. For future wings, an alternate machinable low density foam for tooling should be considered. General Plastics Last-a-Foam FR-7204 is a low density 4 lb/ft^3 polyurethane foam that is very easy to machine. It is commonly used in composite structures as a foam core.

During testing in the wind tunnel, there was also a debonding event of the fiberglass skin from the aft aluminum flap hinge. The fiberglass was the material holding the flaps to the wing. The failure did not cause any loss of components, but an area of several square inches debonded on the upper surface of the wing under compression. The design relies on the 6 aluminum flap sections to hold onto the fiberglass. The comparatively rigid aluminum causes most of the wing bending to happen at the gaps between the flap sections. Buckling of the skin at the gap between flap section 1 and 2, where bending moment is high, caused the debonding (see Figure 39). Bonding the skin to aluminum with epoxy can be challenging. The aluminum surfaces were scuffed with sandpaper and carefully cleaned with acetone prior to bonding. A temporary repair can be made with careful cleaning and re-bonding, as well as installing a fastener into the aluminum. The fastener should ideally have a large flange to provide clamping force on the fiberglass skin. A small reinforcing patch of fiberglass could be added to the area to provide added stiffness to resist buckling.

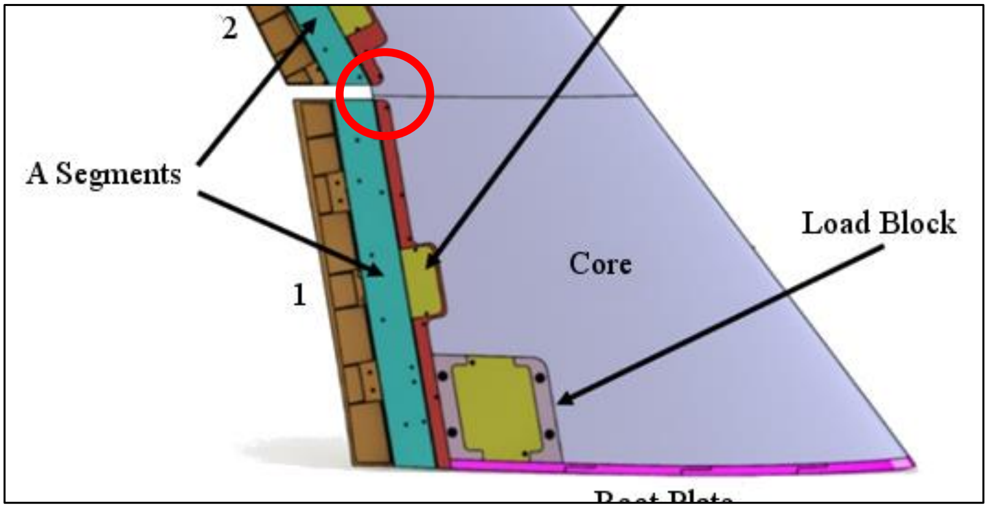

Figure 39: Fiberglass debonding site

Future designs may benefit from using a high-density tooling board, such as General Plastics FR-7120 or OBO Modulan 302, for the flap cove that is bonded to the wing skin. These tooling foams are easy to machine and bond well. This will be more flexible than aluminum, reducing the stress concentrations at the flap gaps in addition to providing a stronger bond to the fiberglass.

Figure 40 shows a comparison of stress distributions in the GTM and CRM wings. The CRM stress distribution shown is at a dynamic pressure of 20 psf and an angle of attack of 1.4 degrees. The GTM-case stress distribution is at 30 psf and an angle of attack of 10 degrees. The figure does not show side by side the most extreme cases for the two wings. Its purpose is to show the different nature of stress distributions, as discussed above. Strength of the CRM wing was demonstrated at 10 psf and 15 psf over a wide range of angles of attack. Multiple cycles of loading and unloading, however, led to debonding between skin and metal hinges that progressed with time and, while not leading to structural failure, may have led to changes in wing stiffness.

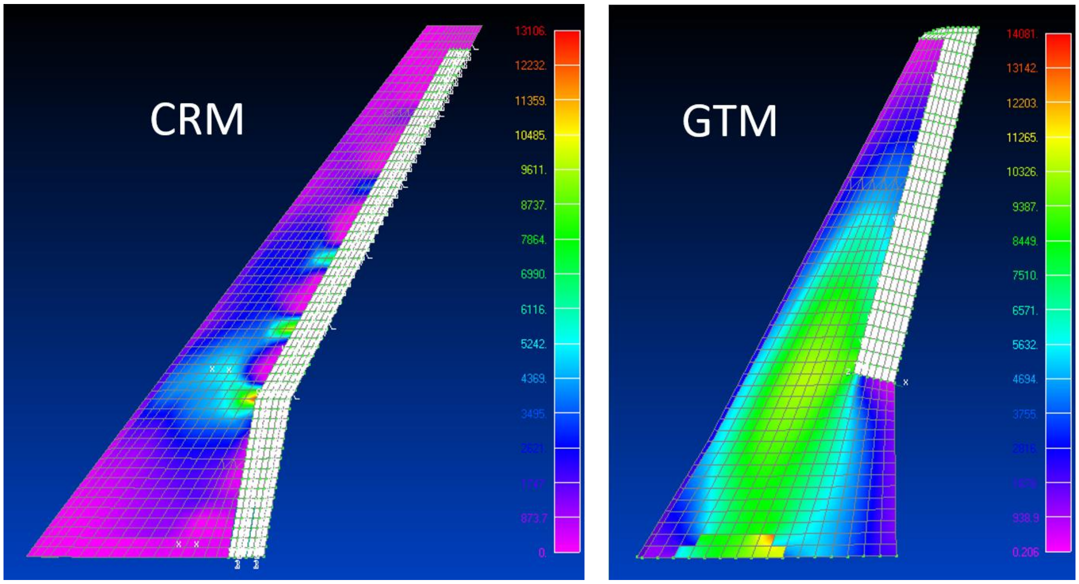

Figure 40: Comparison Analysis of Wind Tunnel Model Stress Distributions

8.2 SERVOS & CONTROLS

The control system was fairly complex and debugging wiring issues and servo failures was very time consuming and hard to solve. Improvements such as consolidating circuitry onto a single PCB would reduce wiring failures and mistakes. Inside the control box, there were often wiring failures due to fatigue in the wires from the encoder counter mezzanine board to the control box panel connectors that plug into the wing. The PCB could have been designed to be soldered directly to the panel connectors, which would reduce the connection to the Arduino to a couple wires consisting of a serial bus and a couple digital lines for serial addressing.

The A7050 thin-wing servos used were high quality and mostly metal, but the design of the lead screw placed axial loads on the shaft of the servo. The servo cap was plastic and cracked on several servos. This could have been a contributing factor to servo burnout. During the first attempt of a wind tunnel test, one servo did burn out, and a wire short created a significant amount of heat that melted the entire wire harness, which had to be replaced. The melted harness could have been prevented if fuses were used. After that initial test, all wiring was replaced and upgraded, and the servos were upgraded to MKS6130 thin wing servos. These servos had slightly more torque, and importantly feature a full aluminum body that proved much more resilient to axial loads. These have proven to be reliable.

The optical encoders worked well once wiring issues were resolved, however the mechanical design of the pinned encoder strip caused binding during actuation. Lead screws had a slight axial misalignment with the axis of rotation, causing a wobble during rotation. The loose tolerances side to side on the driven linkage pin joint (which threads into the lead screw and clamps onto the encoder strip) meant that the encoder strip was being pushed laterally. The alignment track on the cradle with the encoder sensor head constrained the encoder strip laterally. The interference during the wobble caused the encoder strip to warp, introducing measurement nonlinearities and occasional missed counts. It may be possible to use a potentiometer for feedback in a future design, which could be tied into the servo directly and eliminate the need for a microcontroller to close the feedback loop. The challenge with a potentiometer is finding something that fits, has the correct travel, and has low noise. Otherwise, a better mechanical design of the encoder system could solve the difficulty. The encoders are industrial quality, and when installed appropriately can be very robust.

CONCLUSION

The active aeroelastic VCCTEF-wing wind tunnel model developed for tests of in-flight real time wing twist and camber optimization methods is unique from the aeroservoelastic model design as well as aeroservoelastic and MDO perspectives. Construction, shakedown testing, and initial aeroelastic VCCTEF morphing tests have been completed. AIAA conference publication of the work can be found in reference [7]. The model does require some maintenance and minor improvements, based on the experience gained with it to date. It will be available at the University of Washington's Kirsten Wind Tunnel for future testing of active aeroelastic morphing algorithms and will, hopefully, continue to contribute to the development of real-time aeroelastic morphing technology.

BIBLIOGRAPHY

[1] Urnes, J., and Nguyen, N., "A Mission Adaptive Variable Camber Flap Control System to Optimize High Lift and Cruise Lift to Drag Ratios of Future N+3 Transport Aircraft", AIAA Paper 2013-214, 51st AIAA Aerospace Sciences Meeting including the New Horizons Forum and Aerospace Exposition, 2013, DOI: 10.2514/6.2013-214

[2] Precup, N., Mor, M., and Livne, E., "Design, Construction, and Tests of an Aeroelastic Wind Tunnel Model of a Variable Camber Continuous Trailing Edge Flap (VCCTEF) Concept Wing", AIAA Paper 2014-2442, June 2014, AIAA Aviation 2014 Conference, Atlanta, GA, DOI: 10.2514/6.2014-2442

[3] 3. Precup, N., Mor, M., and Livne, E., "The design, construction, and tests of a concept aeroelastic wind tunnel model of a high-lift variable camber continuous trailing edge flap (HL-VCCTEF) wing configuration", 56th AIAA/ASCE/AHS/ASC Structures, Structural Dynamics, and Materials Conference, January 2015, Kissimmee, Florida, AIAA 2015-1406, DOI: 10.2514/6.2015-1406

[4] 4. Nguyen, N., Precup, N., Livne, E., Urnes, J.M., Dickey, E., Nelson, C, Chiew, J., Rodriguez, D.L., Ting, E., and Lebofsky, S., "Wind Tunnel Investigation of a Flexible Wing High-Lift Configuration with a Variable Camber Continuous Trailing Edge Flap Design", AIAA Paper, 2015-2417, 33rd AIAA Applied Aerodynamics Conference, 2015, DOI: 10.2514/6.2015-2417

[5] CRM - https://commonresearchmodel.larc.nasa.gov/)

[6] Vassberg, J., Dehaan, M., Rivers, M., Wahls, M., "Development of a Common Research Model for Applied CFD Validation Studies", 26th AIAA Applied Aerodynamics Conference, 2008, AIAA Paper 2008-6919, DOI: 10.2514/6.2008-6919

[7] Precup, N., Mundt, T. Mor, M., and Livne, E., “An Active Variable Camber Continuous Trailing Edge Flapped Wing Wind Tunnel Model for Aeroelastic “In-Flight” Shape Optimization Tests”, AIAA Paper 2018-3106, June 2018, AIAA Aviation 2018 Conference, Atlanta, GA, DOI: 10.2514/6.2018-3106